Chapter-4

BEHAVIOURS OF ION-ACOUSTIC WAVES IN RELATIVISTIC GYROMAGNETOACTIVE QUANTUM PLASMAS

Abstract: *We report a relativistic quantum hydrodynamic model formalism to investigate the behaviours of ion-acoustic waves excitable in ultra-dense quantum plasma systems. The judicious corrections are considered due to geometric and relativistic effects*[†]*. The model evolves under the conjoint influence of the Coriolis rotation, Lorentz force, electrostatic confinement pressure, quantum Bohm potential, and so forth. A standard normal spherical wave analysis reduces the plasma model into a quartic linear dispersion relation. The significant stabilizing and destabilizing factors are illustratively discussed. A unique zero-growth bouncing point is reported to exist in the wave space for the first time. The implications and application are finally contextualized in real astronomical circumstances.*

4.1 INTRODUCTION

There exist a significant number of realistic spheres extensively dominated by ultra-dense quantum plasmas naturalistically [1-8]. The area of ultra-high density quantum plasmas in one-dimensional regime is one of the most researched fields. Its potential applications range from the terrestrial scales to astrophysical scales of space and time [1-8]. In the laboratory scales, it has important applications in laser plasma based ion-acceleration [1], quantum diodes [2], momentum-resolved tunnelling in quantum wire [3]. Luttinger liquid theory is effectively used to describe one-dimensional quantum fluids in such systems [4]. One-dimensional quantum hydrodynamic model is also used to model the electronic dynamics in quantum wells [5]. In the astrophysical scales, such high-density quantum plasma is widely found in compact astrophysical objects like white dwarfs, brown dwarfs, neutron stars, and so on [8-12].

It is a well-established fact that in ultra-dense quantum plasma systems like white dwarfs, the electron quantum degeneracy pressure far exceeds the classical thermal pressure. Quite a good number of studies are present which report the observed magnetic field range in white dwarfs and pre-white dwarfs to be sufficiently high (~ 10^2

[†]Dasgupta, S. and Karmakar, P. K. Relativistic ion-acoustic waves in electrospherically confined gyromagnetoactive quantum plasmas. *Chinese Journal of Physics*, 76: 299-309, 2022.

G). Likewise, the observed magnetic field in isolated neutron stars is reported to be in the range 10^{11}-10^{15} G. The extremely intense magnetic fields in such compact astronomical fluids significantly modify the mobility of the constitutive charged particles (where gyration radius $\to 0$ as magnetic field $\to \infty$) in such a way that the fluid may essentially be approximated as a one-dimensional model [7, 8]. This geometric condition is consistent and correlative with the atmospheric plasmas of compact astroobjects, such as, brown dwarfs, white dwarfs, neutron stars, and so forth [7, 8]. Most of the bounded astrophysical structures are spherical in shape [9]. So, we, herewith, consider a spherically symmetric geometry of the confined plasma in one-dimensional radial direction only so as to develop a simplified understanding of the underlying dynamical complications as a first step for the first time in this direction. Under such extreme conditions of magnetic field and pressure, the Fermi momentum of the quantum system becomes sufficiently high. As a consequence, the relativity parameter which is the ratio between the "electron Fermi-to-relativistic momentum ratio" given as p_F/mc, becomes sensibly large [12]. The equation of state also gets significantly modified due to inclusion of the relativistic effects [12, 13]. Thus, relativistic effects become of utmost importance in the considered scenario. Besides, rigorous investigations reveal that the electron plasma frequency in such ultra-compact plasmas reduces sensibly at higher density as a vital consequence of the sensible relativistic effects [14]. A good number of investigative studies have been conducted to study the relativistic ion-acoustic waves [15-22] and associated non-linear structures [23-35]. Recent observations in the X-ray and radio frequency bands have reported the dominacy of prominent magnetic activities near the magnetospheres of brown dwarf stars [35-37].

In the proposed work, we consider a gyromagnetoactive relativistic quantum plasma system composed of degenerate electrons and weakly coupled [38] singly charged ions. The system is studied in the fabric of compressible quantum hydrodynamic model formalism [21], but with no self-gravity [39]. It is electrostatically confined in a spherically symmetric geometry. The magnetic field considered in this model limits the fluctuations of the system in a one-dimensional spherically symmetric radial direction. The use of the Fermi-Dirac statistics for electrons enables us to take in to account the degeneracy pressure, by virtue of the Pauli exclusion principle. The

degeneracy pressure results in considerable increase in the Fermi momentum, thereby making the relativity parameter [12] sufficiently high. Unidirectionality and large value of relativity parameter prompts us to consider an equation of state which is similar to that of Chandrasekhar, but essentially that of one directional water-bag distribution [24]. Additionally, we also consider the conjoint effects of the Coriolis rotation, electrostatic confinement pressure (scaling quadratic in density), and quantum diffraction effects given by the Bohm potential. We have sufficient astronomical evidences regarding the active rotational effects and magnetic field in white dwarfs, pulsars [40], and other compact astroobjects [27-29]. Moreover, the electrostatic confinement pressure [25, 26] included in our study has been taken into consideration for the first time. The importance of the electrostatic confinement pressure can be realized from the fact that in compact astroobjects, like white dwarfs, pulsars, neutron stars, etc., the constitutive electrons and ions are usually confined in the system with the interaction of their bipolar electric fields. Thus, there are large mean electric fields contributing appreciably to the resultant pressure of the system, and this is much larger than the thermal pressure exerted by the ions [25, 26]. To increase the efficiency of the proposed model, the quantum diffraction effects have also been included in the current study, which was neglected in most of the previous studies [13-15, 18, 19]. It results in significant modification of the outcomes in the lower wavelength range. These are some of the main novelty factors of the considered study. All the effects considered herein are of great importance in the realistic compact astrocosmic backdrops. The main motivation behind the proposed study is driven by the fact that none of the previous authors has reported any analysis with all the above important active factors taken into account simultaneously in such circumstances as far as seen. More than hundred oscillation modes have already been reported to exist in white dwarfs [27, 32], like PG 1159-035, GD 358, and so forth. It clearly indicates that the ion-acoustic mode kinetics proposed herein under the joint action of various realistic parametric factors will be of extensive relevance in understanding the diversified compact astrophysical instability phenomena.

4.2 PHYSICAL MODEL AND FORMALISM

We propose a relativistic quantum hydrodynamic model to investigate the ion-acoustic wave excitation and propagation in an ultra-dense gyromagnetoactive spherical plasma system. It consists of a quantum-mechanical fluid of tiny electrons and a classical fluid

consisting of heavy ions. The system evolves under the conjoint action of the Coriolis rotation [11], Lorentz force field [19], and degenerate relativistic electronic pressure effects [14, 15]. We also consider the electrostatic confinement pressure effects [25, 26] for the first time as far as seen. Other than this, to increase the efficacy of the model, we also include the quantum diffraction effects by means of the Bohm potential, which is neglected in most of the previous studies [13-15, 18, 19]. The physical model setup adopted here is a weakly coupled plasma system of compact astrophysical relevance [15], validated only on the justifying grounds that, the collision frequency ($\nu_{col} \approx (\ln \Lambda/\Lambda)\omega_{pi}$~$10^{-33}$ Hz; where, $\Lambda = 4\pi\varepsilon_0^{3/2} T^{3/2}/e^3 n_0^{1/2}$ denotes the population number of the constitutive particles in the Debye sphere [38]) is negligibly small with respect to the normal bulk plasma ion-acoustic wave frequency scale ($\omega_{pi} = \sqrt{\mathrm{n}_0 e^2/\varepsilon_0 m_i}$ ~10^6 Hz [15]) in a weakly coupled relativistic system like ours. It implicates, in other words in the customary notations [38] that, the collision time scale (~10^{33} s) supersedes the corresponding bulk plasma ion-acoustic wave time scale (~ 10^{-6} s) on which our model is founded. It hereby means that the interparticle collisions may justifiably be ignored in our analysis in such environs bearing of compact astrophysical relevance. The practical relevancy of such complex bi-ion plasmas can be realized in brown dwarfs, which indeed consist of electrons and *H*-ions, with mass-scaling in the range $0.01 < M_{BD}/M_{\odot} < 0.08$, where $M_{\odot}$ is the solar mass [31, 33]. Similar circumstances dominated by plasma activities can also be found in *He*-white dwarfs, with the mass-scaling ranging as $0.08 < M_{WD}/M_{\odot} < 0.25$ [31, 33]. The basic equations governing the dynamics of the considered system are the flux conservation continuity equation, force-balancing momentum equation and the appropriate equation of state for each of the constituent species along with full relativistic corrections [13-15]. The equations governing the dynamics of the relativistic electronic species, in their customary notations [13, 14], are cast as

$$\partial_t(\gamma_e n_e) + r^{-2}\partial_r(\gamma_e r^2 n_e v_e) = 0, \tag{4.1}$$

$$m_e H(\partial_t + v_e\partial_r)\gamma_e v_e = -\gamma_e n_e^{-1}(\partial_r + v_e c^{-2}\partial_t)P_e + e\partial_r\Phi + \hbar^2(2m_e)^{-1}\nabla\left(\sqrt{n_e}\right)^{-1}\left\{c^{-2}\partial_t^2\sqrt{n_e} - r^{-2}\partial_r\sqrt{n_e}\right\}, \tag{4.2}$$

$$P_e = \left(2m_e^2 c^3\right) h^{-1}\left[\xi\left(\xi+1\right)^{\frac{1}{2}} - \sinh^{-1}\left(\xi\right)\right]. \tag{4.3}$$

Likewise, the equations governing the relativistic classical ionic fluid dynamics are cast as

$$\partial_t\left(\gamma_i\, n_i\right) + r^{-2}\partial_r\left(\gamma_i r^2\, n_i\, v_i\right) = 0, \tag{4.4}$$

$$\left(\partial_t + v_i\partial_r\right)\gamma_i v_i = -em_i^{-1}\,\partial_r\Phi - 2\Omega_\phi v_{hi\theta} - eB_\phi\left(m_i\right)^{-1} v_{hi\theta} - \left(m_i n_i\right)\partial_r P_i, \tag{4.5}$$

$$P_i = \gamma_i C_p n_i^2. \tag{4.6}$$

The electrostatic Poisson equation is given in customary notations [13-15] as

$$r^{-2}\partial_r\left(r^2\partial_r\,\Phi\right) = e\varepsilon_0^{-1}\left(\gamma_e\, n_e - \gamma_i\, n_i\right). \tag{4.7}$$

The notations, $n_{e(i)}$ and $v_{e(i)}$, denote the mass-weighted average population density and the mass-weighted average velocity of the electrons (ions) with their inertial mass $m_{e(i)}$, respectively. $\gamma_{e(i)} = \left(\sqrt{1 - v_{e(i)}^2/c^2}\right)^{-1}$ are their respective relativistic dilation factor. In equation (4.2), $H = \sqrt{1+\xi^2}$ is the non-dimensional enthalpy density of the constitutive degenerate electrons [13, 14, 15, 21]. Here, $\xi = h n_e / 4 m_e c$ designates the electronic relativistic quantum action-to-momentum ratio. The term, $C_F = 2\Omega_\phi v_{hi\theta}$, stands the Coriolis rotational force [11], with Ω_ϕ denoting the azimuthal component of the angular velocity and $v_{hi\theta}$ designating the polar component of the rotational velocity of the inertial ionic fluid. $\omega_{gi} = e B_\phi / m_i$ is the magnetic gyrofrequency for the relativistic ionic species, where B_ϕ is the magnetic field acting along the azimuthal direction. C_p is a constant of proportionality known as the polytropic constant associated

with the electrostatic confinement pressure of the ionic fluid. The electronic charge is given as $e=1.6\times10^{-19}C$.

A number of points regarding the above equations are noteworthy. Equation (4.1) denotes the continuity equation for the electronic flux conservation. Equation (4.2) represents the force-balancing momentum equation for the electronic dynamics where forces due to the relativistic inertial motion (L.H.S), relativistic quantum-degeneracy pressure (1st term in R.H.S), electrostatic potential (2nd term in R.H.S), and Bohm potential (3rd term in R.H.S) exactly balance each other. It may be noted that the Coriolis rotational force for the electronic species, $C_{Fe}=2m_e\left(v\times\omega\right)$, is extremely small owing to their negligibly small mass. Additionally, the most pronounced effect of the magnetic field on electrons is on their spin dynamics. The spin dynamical evolution of the electrons is not included in our model setup. Hence, the Coriolis rotational force term and the magnetic field term are neglected in the force balancing momentum equation of the electrons (equation (4.2)). However, the effects of the intense magnetic field in restricting the motion of the electronic species to an essentially one-dimensional motion are accounted for with the help of an appropriately modified equation of state. Equation (4.3) is the equation of state that is modified appropriately for the relativistic electronic dynamics in an ultra-dense quantum plasma system [13, 14, 15, 21, 24]. Likewise, equation (4.4) is the analog of equation (4.1), but for the ionic species. Equation (4.5) for the ionic species forms an exact analog of equations (4.2), but with the Coriolis force (2nd term in R.H.S), Lorentz force (3rd term in R.H.S), and electrostatic confinement force (4th term in R.H.S) contributions incorporated in equation (4.5) afresh. The equation of state for the ionic species is given by equation (4.6), where, quite clearly, the confinement pressure scales quadratically with the ionic density [25, 26]. The model equations are closed with the help of the electrostatic Poisson equation, equation (4.7), describing the electrostatic potential distribution developed due to the local charge density fields of the plasma charged species.

We now apply a standard astronormalization scheme [13, 14, 15] in equations (4.1)-(4.7) for a scale invariant analysis of the basic set of governing equations. The dimensionless set of equations are respectively cast as

$$\partial_\tau\left(\gamma_e^*\,N_e\right)+R^{-2}\,\partial_R\left(\gamma_e^*\;R^2N_e\,M_e\right)=0\,, \tag{4.8}$$

$$m_e m_i^{-1}\left(1+\xi_0^2 N_e^2\right)^{\frac{1}{2}} N_e\left(\partial_\tau + M_e\partial_R\right)\gamma_e^* M_e = -\gamma_e^* 2^{-1}\left[\left(1-\xi_0\right)\xi_0^{-2}\left(\partial_R N_e + M_e\alpha\partial_\tau N_e\right)\right.$$
$$\left. + 2^{-1}\left(3+\xi_0\right)\left(N_e^2\,\partial_R N_e + M_e\alpha N_e^2\partial_\tau N_e\right)\right] + N_e\partial_R\Phi_E$$
$$-2^{-1} m_e m_i^{-1} H_p^2\alpha^{-2}\left[2^{-1}\partial_R^3 N_e + R^{-1}\partial_R^2 N_e - R^{-2}\partial_R N_e\right], \quad (4.9)$$

$$\partial_\tau\left(\gamma_i^* N_i\right) + R^{-2}\,\partial_R\left(\gamma_i^* R^2 N_i M_i\right) = 0\,, \quad (4.10)$$

$$N_i\left(\partial_\tau + M_i\partial_R\right)\gamma_i^* M_i + N_i\partial_R\Phi_E + 2N_i C_F^* + N_i\,\Omega_{gi}^* M_{hi\theta} + 2^{-1}\partial_R\left(\gamma_i^* C_p^* N_i^2\right) = 0, \quad (4.11)$$

$$R^{-2}\,\partial_R\left(R^2\partial_R\Phi_E\right) = e\left(\gamma_e^* N_e - \gamma_i^* N_i\right). \quad (4.12)$$

In our normalized system [13, 14, 15, 22], the spatial radial coordinate, *r*, is now rescaled as $R = r/L_0$; where, $L_0 = c_s/\omega_{pi}$ is a characteristic spatial scale termed as the ion-acoustic wave scale length. The temporal coordinate, *t*, rescales as $\tau = t/\omega_{pi}^{-1}$, where $\omega_{pi} = \sqrt{n_0 e^2/\varepsilon_0 m_i}$ designates the ion plasma oscillation frequency. Similarly, $c_s = \sqrt{2E_{Fe}/m_i}$ is the ion-acoustic phase speed in terms of the electronic Fermi energy. $E_{Fe} = p_F^2/2m_e$, with $p_F = h n_0/4$ as the corresponding Fermi momentum. The rescaled electronic (ionic) population density is given as $N_{e(i)} = n_{e(i)}/n_0$, where n_0 is the linear particle concentration in our radial one-dimensional problem. The normalized magnetic gyrofrequency is given as $\Omega_{gi}^* = \omega_{gi}/\omega_{pi}$. $M_{e(i)} = v_{e(i)}/c_s$ gives the Mach number of the electronic (ionic) species. The normalized relativistic dilation factor is given as $\gamma_{e(i)}^* = \left(1-\alpha M_{e(i)}^2\right)^{-1/2}$ for both the considered relativistic species. The quantum parameter, $H_p = \hbar/\left(m_e c L\right)$, gives the ratio of the plasmon energy to the Fermi energy. Then, $\alpha = c_s^2/c^2 = m_e\,\xi_0^2/m_i$ where $\xi_0 = p_F/\left(m_e c\right)$ is the electronic relativity parameter. $C_F^* = \Omega_\phi^* M_{hi\theta}$ gives the rescaled Coriolis rotation. The azimuthal component of angular velocity and the polar component of rotational velocity are

normalized as $\Omega_{\phi}^{*}=\Omega_{\phi}/\omega_{pi}$ and $M_{hi\theta}=v_{hi\theta}/c_s$, respectively. $\Omega_{gi}^{*}M_{hi\theta}$ gives the normalized Lorentz force field. The constant of proportionality in the electrostatic confinement pressure, as given by equation (4.6), is rescaled as $C_p^{*}=C_p n_0/E_{Fe}$. Lastly, $\Phi_E=e\Phi/(2E_{Fe})$ appearing in equation (4.12) is the normalized electrostatic potential on the Fermi potential scale.

4.3 LINEAR STABILITY ANALYSIS

We linearly perturb the relevant plasma parameters (F_1) appearing in equations (4.8)-(4.12) about their homogeneous equilibrium values (F_0) by using a standard normal spherical mode analysis in an auto-normalized Fourier transformed wave space as

$$F(R,\tau)=F_0+F_1=F_0+R^{-1}F_{10}\exp\left[-i\left(\Omega\tau-k^{*}R\right)\right], \tag{4.13}$$

$$F=\left[N_s \quad M_s \quad \Phi_E\right]^T, \tag{4.14}$$

$$F_0=\left[1 \quad 0 \quad 0\right]^T, \tag{4.15}$$

$$F_1=\left[N_{s1} \quad M_{s1} \quad \Phi_{E1}\right]^T. \tag{4.16}$$

Here, Ω $(=\omega/\omega_{pi})$ denotes the normalized fluctuation frequency and k^{*} $(\sim k/L_0^{-1})$ designates the normalized wavenumber. *F1* denotes the considered fluctuations of the physical variables *F* on a linear scale, over the equilibrium fluid parameters, *F0*. It may be pertinent here to mention that the seed perturbation, as given in equation (4.13), could be sourced due to the available free energy associated with the initial inhomogeneities in the diversified constitutive parametric local density fields. In the new Fourier wave space (Ω, k^{*}), the linear spatial and temporal operators get self-consistently transformed as $\partial/\partial R\rightarrow\left(ik^{*}-1/R\right)$ and $\partial/\partial\tau\rightarrow(-i\,\Omega)$, respectively. Evidently, the term $1/R$ appears in equation (4.13) as a geometric modulating factor, appearing due to the deviation from the plane-parallel geometrical approximation. It

shows how a Fourier wave spectral component (exponential term) gets modified due to non-planar geometric effects (curvature term). Most of the astronomical bounded systems are evidently found to have spherical structure because of the long-range inward self-gravity [9]. Thus, spherical mode analysis enhances the accuracy of the obtained results and increases its corresponding relevance in relation to the actual astrocosmical scenarios. However, the prime demerit of the aforesaid analysis lies in the time consuming arithmetic calculations due to the increase in number of terms having $1/R$-dependencies. The linearly perturbed relevant physical parameters from equations (4.8)-(4.12) in the new wave space can respectively be cast as

$$N_{e1}=-i\Omega^{-1}\left(ik^{*}+R^{-1}\right)M_{e1}\,, \tag{4.17}$$

$$M_{e1}=\left(ik^{*}-R^{-1}\right)\left[-i\Omega m_e m_i^{-1}\left(1+\xi_0^{2}\right)^{\frac{1}{2}}-i(2\Omega)^{-1}\left(k^{*^2}+R^{-2}\right)\left(-A+2^{-1}m_e m_i^{-1}H_p^{2}\alpha^{-2}k^{*^2}\right)\right]^{-1}\Phi_{E1}, \tag{4.18}$$

$$N_{i1}=-i\Omega^{-1}\left(ik^{*}+R^{-1}\right)M_{i1}, \tag{4.19}$$

$$M_{i1}=\left(ik^{*}-R^{-1}\right)\left[-i\Omega-i\Omega^{-1}\left(ik^{*}+R^{-1}\right)\left(2C_F^{*}+\Omega_{gi}^{*}M_{hi\theta}\right)+i\Omega^{-1}C_p^{*}\left(k^{*2}+R^{-2}\right)\right]^{-1}\Phi_{E1}. \tag{4.20}$$

where, $A=\left[\xi_0^{-1}\left(\xi_0^{-1}-1\right)+(2)^{-1}3\left(1+\xi_0\right)\right].$ (4.21)

After performing the relevant algebraic procedures of elimination and substitution, we arrive at a linear generalized quartic dispersion relation cast as

$$A_4\Omega^{4}+A_2\Omega^{2}+A_0=0. \tag{4.22}$$

The different coefficients appearing in equation (4.22) are given as

$$A_4=\left[m_e m_i^{-1}k^{*^2}\left(1+\xi_0^{2}\right)^{\frac{1}{2}}\right]; \tag{4.23}$$

$$A_2 = \left[m_e m_i^{-1} \left(1+\xi_0^2\right)^{\frac{1}{2}} \left\{P - \left(k^{*2} + R^{-2}\right)\left(C_p^* + 1\right)\right\} + \left(k^{*2} + R^{-2}\right)\left((2)^{-1} Q - 1\right)\right]; \tag{4.24}$$

$$A_0 = \left[(2)^{-1} Q\left(k^{*2} + R^{-2}\right) \left\{P - \left(k^{*2} + R^{-2}\right)\left(C_p^* + 1\right)\right\} - \left(k^{*2} + R^{-2}\right)P\right]. \tag{4.25}$$

The substituted parameters in equations (4.23)-(4.25) in an expanded form are given as

$$P = \left(ik^* + R^{-1}\right)\left(2C_F^* + \Omega_{gi}^* M_{hi\theta}\right); \tag{4.26}$$

$$Q = \left(-A + (2)^{-1} m_e m_i^{-1} H_p^2 \alpha^{-2} k^{*2}\right). \tag{4.27}$$

In the present semi-analytic investigation, we are interested to study only the low-frequency ion-acoustic modes. Thus, ignoring all powers of Ω higher than 2 as per the traditional approach, we obtain the modified dispersion relation as

$$A_2 \Omega^2 + A_0 = 0. \tag{4.28}$$

which, in turn, gives

$$\Omega = i \left[(2)^{-1} Q\left(k^{*2} + R^{-2}\right) \left\{P - \left(k^{*2} + R^{-2}\right)\left(1 + C_p^*\right)\right\} - \left(k^{*2} + R^{-2}\right)P\right]^{+\frac{1}{2}}$$
$$\times \left[m_e m_i^{-1} \left(1+\xi_0^2\right)^{\frac{1}{2}} \left\{P - \left(k^{*2} + R^{-2}\right)\left(1 + C_p^*\right)\right\} + \left(k^{*2} + R^{-2}\right)\left((2)^{-1} Q - 1\right)\right]^{-\frac{1}{2}}. \tag{4.29}$$

Now, for the instability analysis, we split Ω in the L.H.S of equation (4.29) as $\Omega_r + i\Omega_i$ [21], where Ω_r and Ω_i denote the real (regular) and imaginary (irregular) parts of Ω, respectively. It may be noteworthy that the positive value of Ω_i gives the instability growth rate; whereas, its negative value measures the instability damping rate. Thus, on comparing the real and imaginary parts from both sides of equation (4.26), we find that only Ω_i survives. It is clearly seen from equation (4.29) that the

ion-acoustic instability behaviour sensitively depends on the several important parameters considered herein like the relativity parameter, Coriolis force, Lorentz force field, quantum parameter, and so on.

4.4 RESULTS AND DISCUSSIONS

A semi-analytic investigation is put forward to study the relativistic ion-acoustic waves excitable in compact astrophysical structures like brown dwarfs, white dwarfs, etc. We consider a two-component plasma system comprising of electronic and ionic fluid. The ion-acoustic mode sustains because of the restoring force provided by the electronic species, and the inertial force provided by the weakly coupled heavier singly charged ionic species. The dynamics of the complex plasma system is modelled with the help of a quantum hydrodynamic formalism in a spherically symmetric geometry with perturbations along the radial direction. The system evolves under the conjoint influence of the Coriolis rotation, Lorentz force field, electrostatic confinement pressure, and quantum diffraction effects given by the Bohm potential, and so on in an ultra-dense plasma environment. After a systematic linear normal mode analysis, we derive a generalized linear quartic dispersion relation with atypical coefficients (equation (4.28)). A numerical illustrative platform is provided for this dispersion analysis to yield the various ion-acoustic results as displayed in figures 4.1- 4.6. In the obtained scale-free figures 4.1-4.6, k^* signifies a broader space of the auto-normalized wavenumber, $k^* = k/2\pi L_0^{-1}$, as per the adopted Fourier transformation (equation 4.13). Accordingly, the hydrodynamic regime is characterized by a subcritical angular wavenumber defined as $k^* = k/2\pi L_0^{-1} < 1$. In this purview, the kinetic regime is characterized by a supercritical wavenumber, specified as: $k^* = k/2\pi L_0^{-1} > 1$. The hybrid (hydrokinetic) class of intermediate collective fluctuations is described by a transcritical wavenumber, $k^* = k/2\pi L_0^{-1} \approx 1$. It is noteworthy to mention here that the different input values employed in our numerical study correspond to realistic compact astronomic circumstances as depicted in the literature [14, 15, 22, 28].

In figure 4.1, we depict the profile structure of the normalized growth rate (Ω_i) with variation in the normalized wavenumber (k^*) for different values of the Coriolis rotational force (C_F^*). The various input values used herein are: $\xi_0 = 0.4835$ [15],

$C_p^* = 4$ [26], $H_p = 0.1$ [22], $\alpha = 1.27 \times 10^{-4}$ [15]. We estimate R = 10^4 , with the calculated value of $\omega_{pi} \sim 10^6$ Hz, $c_s \sim 10^6$ m s^{-1}, $L_0 = c_s / \omega_{pi} \sim 1$ m, $r = R_* \sim 10$ km [31] so as to correspond to real astronomic circumstances. We further find that $\Omega_{gi}^* = \omega_{gi} / \omega_{pi} \sim 10^3$ with $\omega_{gi} = e B_\phi / m_i \sim 10^9$ Hz for a mean $B_\phi = 10$ T [11] linking to the same astronomic configurations. The different coloured lines link to $C_F^* = 50$ (blue solid line), $C_F^* = 100$ (red dashed line), and $C_F^* = 150$ (black dotted line). It is clearly seen that, for a particular value of the C_F^*, the instability growth rate of the system gradually increases from zero, reaches the maximum and then finally goes back to zero at a certain k^* (zero growth-bouncing point) with a strong propensity to increase again. As the value of the C_F^* increases, it is seen that the zero growth-bouncing point shifts towards the lower-k^* region. It is found that, as C_F^* increases, the growth rate of the wave increases in the wave-space defined by $k^* = 0 - 15$. It can be attributed to the fact that an increase in the Coriolis rotation leads to an increase in the rotational kinetic energy ($E_r = (1/2) I \omega_r^2$, where *I* is the moment of inertia around the axis of rotation, and ω_r is the rotational velocity of the system), and vice-versa. It is known that $I = MK_g^2$, where *M* is the net mass and K_g is the radius of gyration around the rotation axis of reference. Thus, higher the mass, higher the moment of inertia, higher the rotational kinetic energy, and higher is the resulting Coriolis rotation. It is an established fact that higher the mass of such systems, higher the possibility for exciting their gravitational instabilities. Thus, an enhancement in the Coriolis rotation increases the ion-acoustic wave growth (as a destabilizing agency), and vice-versa (figure 4.1(a)). This result is fairly consistent with the previously reported astronomical observations [28]. In this particular context, white dwarfs, such as U Geminorum, OY Car, etc., clearly indicate that collapsing dwarf stars having greater mass rotate faster, and vice-versa [28]. There is a growth bouncing effect on the wave-space (figure 4.1(b)), which can be attributed to the quantum diffraction effects which come into the picture due to the consideration of the Bohm potential term. Figure 4.2 shows a colourspectral pattern profile of the same variation with *R* as an additional parameter for a fixed $C_F^* = 100$.

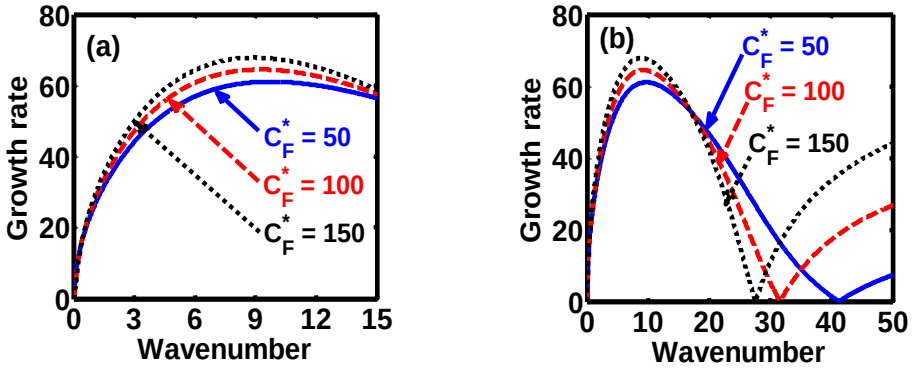

Figure 4.1: *Profile of the normalized growth rate* (Ω_i) *of the ion-acoustic wave with variation in the normalized wavenumber* (k^*) *for the different indicated values of the Coriolis rotational force* (C_F^*)*. The distinct panels depict the same in the domains: (a)* $k^*=0-15$ *and (b)* $k^*=0-50$.

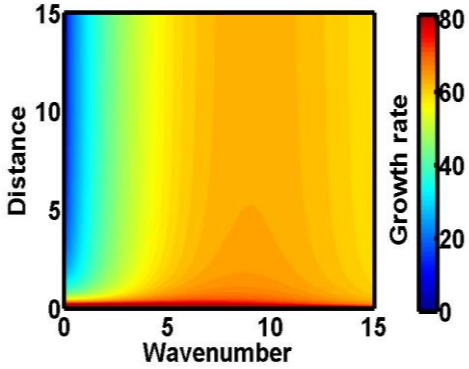

Figure 4.2: *Colourspectral profile of the normalized growth rate* (Ω_i) *of the ion-acoustic wave with variation in the normalized spatial coordinate* (R) *and normalized wave number* (k^*) *for a fixed value of the Coriolis rotational force* $(C_F^*=100)$.

In figure 4.3, we show the same as figure 4.1, but for the different values of the normalized magnetic gyrofrequency (Ω_{gi}^*). The various coloured lines correspond to $\Omega_{gi}^*=1000$ (blue solid line), $\Omega_{gi}^*=2000$ (red dashed line), $\Omega_{gi}^*=3000$ (black dotted line). A trend similar to that of figure 4.1 is observed for a particular Ω_{gi}^*. It is noticed that, as Ω_{gi}^* increases, the zero growth-bouncing point shifts towards the higher-k^*

regime. It is clearly seen that increasing Ω_{gi}^{*} increases the growth rate of the system in the k^{*} range defined by k^{*} = 0-15 (figure 4.3(a)), thereby allowing the ion-acoustic instability to grow sensibly. Usually, it is seen that an increase in the magnetic field and hence, magnetic gyrofrequency enhances the degree of particle confinement. However, figure 4.3(a) depicts exactly the opposite features. The magnetic gyrofrequency is directly related to the velocity of the constitutive particles. Thus, increase in the magnetic gyrofrequency leads to an enhanced particle velocity, thereby causing its escape from the natural magnetic confinement effects. In our relativistic system, the escape of particles from the magnetic confinement becomes more pronounced due to the pre-existing relativistic velocities. An analogy that could be drawn here is the escape of an artificial satellite from the planetary (geo) gravitational confinement when it attains the escape velocity. The satellite cannot escape the gravitational confinement with any given random velocity. If and when the satellite reaches the escape velocity, it breaks the gravitational confinement and gets free to move out of its influence. Thus, the enhancing magnetic gyrofrequency increases the ion-acoustic growth rate, thereby destabilizing the system under consideration. In other words, the escape of the relativistic ions from the magnetic confinement results in an enhanced growth rate. In figure 4.3(b), after the phase bouncing at the zero growth-bouncing point, the Ω_{gi}^{*} effect on the growth gets reversed, that is, the growth rate corresponding to $\Omega_{gi}^{*}=1000$ is the highest, followed by the lower ones ($\Omega_{gi}^{*}=2000$, and $\Omega_{gi}^{*}=3000$). Similarly, figure 4.4 shows the same spectral profile as figure 4.2, but for $\Omega_{gi}^{*}=2000$. The main difference noticed here (figure 4.4) is that the lowest growth occurs in a closer proximity to the centre than the previous case (figure 4.2), and so forth.

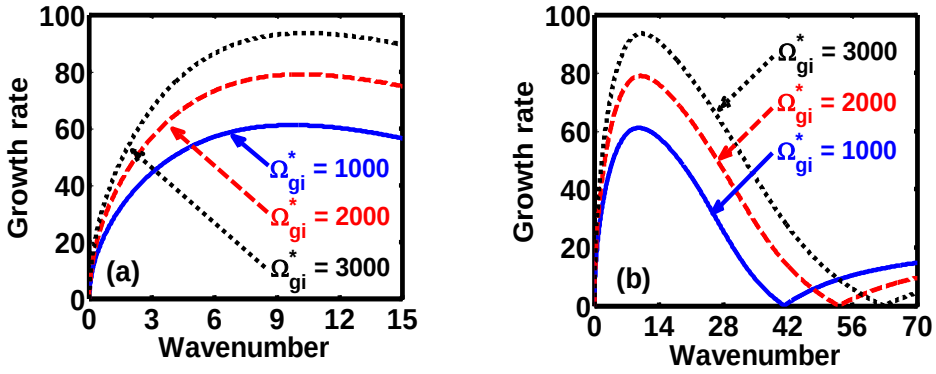

Figure 4.3: *Same as figure 4.1, but for the different indicated values of the normalized magnetic gyrofrequency* $\left(\Omega^*_{gi}\right)$. *The distinct panels depict: (a)* $k^*=0-15$ *and (b)* $k^*=0-70$.

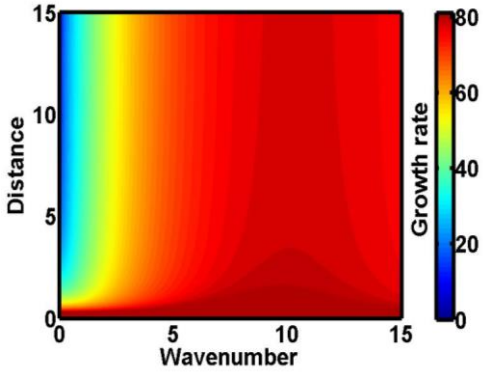

Figure 4.4: *Same as figure 4.2, but for a fixed value of the normalized magnetic gyrofrequency* $\left(\Omega^*_{gi}=2000\right)$.

In figure 4.5, we depict the same as figure 4.1, but for different values of the equilibrium linear ionic concentration $\left(n_0\right)$. The different lines correspond to $n_0=4\times10^{11}$ m^{-1} [13] (blue solid line), $n_0=8\times10^{11}$ m^{-1} [15] (red dashed line), $n_0=1\times10^{12}$ m^{-1} [13] (black dotted line). For a fixed n_0, it follows the same pattern (figure 4.5(b)) as that of the previous C^*_F-case (figure 4.1(b)). However, as n_0 increases, zero growth-bouncing point shifts towards the lower-k^* region. In the lowest-k^* limit (k^*=0-6), the instability growth increases with n_0 (figure 4.5(a)). As the wave progresses (k^*=6-15), the confinement pressure achieves an appreciable value, resulting in growth reduction with increase in n_0 (figure 4.5(a)). After the phase-

bouncing due to quantum diffraction effects, the n_0-dependency of the growth gets just reversed (figure 4.5(b)), as found before (figure 4.5(a)). This can possibly be traced back to the mutual coupling of the diffraction effects with the ionic confinement. Lastly, figure 4.6 shows the same behaviour as figure 4.2, but for $n_0 = 4\times10^{11}$ m^{-1}. The only disparity noticed here as compared to the previous case (figure 4.2) is in the shifting of the lowest growth in an anti-centric-ward direction.

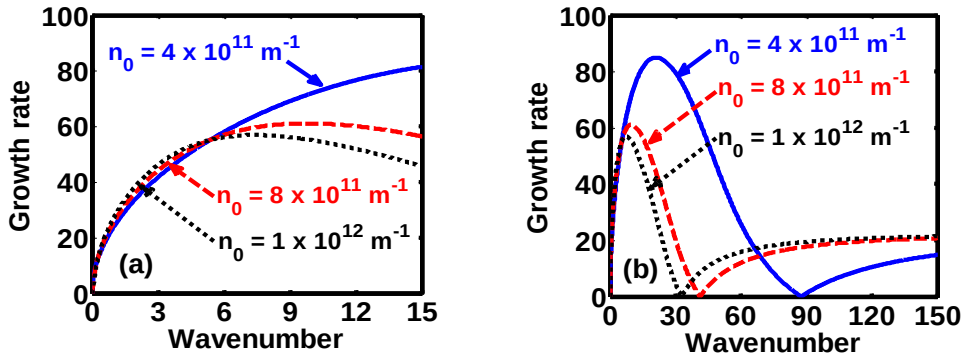

Figure 4.5: *Same as figure 4.1, but for the different indicated values of the equilibrium linear ionic concentration* (n_0)*. The distinct panels depict the above in: (a)* $k^* = 0-15$ *and (b)* $k^* = 0-150$.

It may be repeated here that none of the previous investigations done in this field [15-23] has considered all the concurrent realistic unavoidable effects simultaneously as proposed herein so as to see a comparative and supportive glimpse of our explored outcomes. Additionally, the electrostatic confinement pressure and gyromagnetoactivity are included in this study for the first time. The quantum diffraction effects had earlier been neglected in most studies related to relativistic ion-acoustic wave instability dynamics [13-15, 18, 19]. The consideration of quantum diffraction effects is another novelty against the previous studies [13-15, 18, 19]. As a consequence, the proposed spherical model analysis seems to go closest to real astrocosmic scenarios. The insufficiency of reported data in the literature may find it difficult to concretely and observationally support the existence of the ion acoustic-zero growth-bouncing points as investigated here. The proposed methodical analysis, despite facts and faults, should have wide-range applicability to explore the diversified wave modes of compact

astroobjects and their circumvent atmospheres in an asteroseismic perspective extensively useful in probing their interior structures.

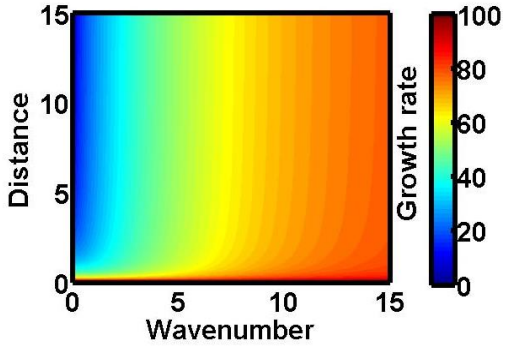

Figure 4.6: *Same as figure 4.2, but for a fixed value of the equilibrium linear ionic concentration* $\left(n_0 = 4\times10^{11}\, m^{-1}\right)$.

4.5 CONCLUSIONS

In this Chapter we propose a relativistic gyromagnetoactive quantum plasma fluid model to investigate the dynamics of the ion-acoustic mode in a spherical geometry. It considers the constitutive ionic dynamics to evolve under the conjoint action of relativistic effects, electrostatic confinement effects, etc. The quantum-mechanical degenerate pressure and quantum diffraction effects are retained only in the electronic dynamics.

In our normal spherical mode analysis, the effects of wave reflection from the plasma-confining boundaries are excluded for the sake of analytic simplicity only. It could be included by adding appropriate Fourier spectral components with opposite phase arguments to the usual Fourier spectral parameters in our formalism to explore the boundary reflection influences (geometric mirror effects) on the ionic modal propagatory dynamics. The formalism in the presence of the plasma boundary reflection effects could resemble the solar acoustic-cavity resonator (huge spherical fireball) exhibiting a plethora of standing non-propagatory wave spectral patterns in addition to the normal gravito-acoustic propagatory modes excited via the gravito-electrostatic sheath (GES) action [39]. Nevertheless, it would be significantly modified with the inclusion of various modal quantum numbers likely to appear in the characteristic spectral patterns under exploration.

The restoring force is provided here by the relativistic degenerate electronic species, governed by an appropriate equation of state of water-bag distribution law [24]. Heavy relativistic singly charged ionic species, confined electrostatically within the system, provide the inertial force for sustaining the ion-acoustic mode. A standard normal spherical mode analysis yields a generalized quartic linear dispersion relation with multiparametric coefficients. A numerical illustrative platform depicts the diverse microphysical aspects of the growth dynamics of the ion-acoustic mode in realistic astrophysical circumstances.

The Coriolis rotation and magnetic field increase the growth of the ion-acoustic mode in the lower wavenumber $\left(k^{*}\right)$ region (figures 4.1(a), 4.3(a)). Thus, the rotation and the field behave as its destabilizing agencies in this k^{*} range. Interestingly, a zero-growth bouncing point is found in both the cases in the higher-k^{*} region (figures 4.1(b), 4.3(b)). It can be physically attributed to the effect of the electronic quantum diffraction. It may be worthwhile that this rotational destabilization aspect is interestingly in good agreement with the previously recorded astronomical observational data on the white dwarfs (U Geminorum, OY Car, etc.), which, in fact, clearly indicate that collapsing dwarfs having greater mass rotate faster, and vice-versa [28]**.** Figures 4.2 and 4.4 display the colourspectral profiles of the growth rate for the variation in the Coriolis rotation and magnetic field in a space defined by radial distance and k^{*}, respectively. In figure 4.5 (a), the linear equilibrium ionic concentration first destabilizes the system in the low-k^{*} regime. However, the electrostatic confinement pressure attains an appreciable value as we move towards the high-k^{*} regime, thereby reversing the influence of the ionic concentration. That is, the linear equilibrium ionic concentration destabilizes the system. As we proceed further in the wavenumber space, we come across the zero-growth bouncing point (figure 4.5(b)). Figure 4.6 displays the colourspectral profile for a fixed value of ionic concentration.

It is finally admitted herewith that the realistic effects considered in our study would exhibit their full influence on the ion-acoustic mode dynamics in diversified plasma parametric windows more prominently in a systematic non-linear analysis executed in similar circumstances. In this direction, the ion-acoustic modes of similar pattern have been predicted to exist in the atmospheres of white dwarfs, neutron stars, and so forth [7]. Also, the discovery of several pulsational modes in progenitors and

white dwarfs (PG 1159-035, GD 358) [27, 32] indicates the opening of a hotspot area of future research in the direction of the ion-acoustic modal signatures. It is in good accord with those explored in our current study as well. It hereby establishes fair correlations and consistencies of our asteroseismic ion-acoustic modal stability analysis investigated here in the realistic compact astronomical circumstances dominated by interdependent quantum plasma effects collectively.

REFERENCES

[1] Macchi, A., Cattani, F., Liseykina, T. V., and Cornolti, F. Laser acceleration of ion bunches at the front surface of overdense plasmas. *Physical Review Letters*, 94(16): 165003, 2005.

[2] Shukla, P. K. and Eliasson, B. Nonlinear theory for a quantum diode in a dense Fermi magnetoplasma. *Physical Review Letters*, 100 (3)**:** 036801, 2008.

[3] Barak, G., Steinberg, H., Pfeiffer, L. N., West, K. W., Glazman, L., Oppen, F. V., and Yacoby, A. Interacting electrons in one dimension beyond the Luttinger-liquid limit. *Nature Physics*, 6: 489-493, 2010.

[4] Imambekov, A. and Glazman, L. I. Universal Theory of Nonlinear Luttinger Liquids. *Science*, 323(5911): 228-231, 2009.

[5] Haas, F., Manfredi, G., Shukla, P. K., and Hervieux, P. A. Breather mode in the many-electron dynamics of semiconductor quantum wells. *Physical Review B*, 80(7):073301, 2009.

[6] Mamun, A. A., Amina, M., and Schlickeiser, R. Nucleus-acoustic shock structures in a strongly coupled self-gravitating degenerate quantum plasma. *Physics of Plasmas*, 23:094503, 2016.

[7] Canuto, V. and Ventura, J. Quantum theory of the dielectric constant of a magnetized plasma and astrophysical applications. *Astrophysics and Space Science*, 18:104-120, 1972.

[8] Carbonaro, P. The degenerate Fermi gas in relativistic fluid dynamics. *Nuovo Cimento B*, 103(5):485-496, 1989.

[9] Bini, D., Cherubini, C., and Filippi, S. Effective geometry of a white dwarf. *Physical Review D*, 83(6):064039, 2011.

[10] Shukla, P. K. and Eliasson, B. Nonlinear aspects of quantum plasma physics. Physics Uspekhi, 53(1): 51-76, 2010.

[11] Ferrario, L. and Wickramasinghe, D. T. Magnetic fields and rotation in white dwarfs and neutron stars. *Monthly Notices of the Royal Astronomical Society*, 356(2):615-620, 2005.

[12] Salpeter, E. E. Energy and pressure of a zero-temperature plasma. *The Astrophysical Journal*, 134(3): 669-682, 1961.

[13] McKerr, M., Haas, F., and Kourakis, I. Ion-acoustic envelope modes in a degenerate relativistic electron-ion plasma. *Physics of Plasmas*, 23:052120, 2016.

[14] Kourakis, I., McKerr, M., Elkamash, I. S., and Haas, F. New insight into the dispersion characteristics of electrostatic waves in ultradense plasmas: electron degeneracy and relativistic effects. *Plasma Physics and Controlled Fusion*, 59(10): 105013, 2017.

[15] McKerr, M., Haas, F., and Kourakis, I. Relativistic theory for localized electrostatic excitations in degenerate electron-ion plasmas. *Physical Review E*, 90 (3):033112, 2014.

[16] Rahman, A. and Ali, S. Solitary and rogue waves in Fermi-Dirac plasmas: relativistic degeneracy effects. *Astrophysics and Space Science*, 351:165-172, 2014

[17] Chandrasekhar, S. Highly collapsed configurations of a stellar mass. *Monthly Notices of the Royal Astronomical Society*, 95(3): 207-225, 1935.

[18] Haas, F. and Kourakis, I. Nonlinear hydrodynamic Langmuir waves in fully degenerate relativistic plasma. *Plasma Physics and Controlled Fusion*, 57(4)**:**044006, 2015.

[19] Behery, E. E., Haas, F., and Kourakis, I. Weakly nonlinear ion-acoustic excitations in a relativistic model for dense quantum plasma. *Physical Review E*, 93(2):023206, 2016.

[20] Haas, F. Modelling of relativistic ion-acoustic waves in ultra-degenerate plasmas. *Journal of Plasma Physics*, 82(6):705820602, 2016.

[21] Elkamash, I. S., Haas, F., and Kourakis, I. Ion-beam/plasma modes in ultradense relativistic quantum plasmas: Dispersion characteristics and beam-driven instability. *Physics of Plasmas*, 24:092119, 2017.

[22] Atteya, A., Behery, E. E., and El-Taibany, W.F. Ion acoustic shock waves in a degenerate relativistic plasma with nuclei of heavy elements. *European Physical Journal Plus*, 132:109, 2017.

[23] Soltani, H., Mohsenpour, T., and Sohbatzadeh, F. Obliquely propagating quantum solitary waves in quantum-magnetized plasma with ultra-relativistic degenerate electrons and positrons. *Contributions to Plasma Physics*, 59(9):e201900038, 2019.

[24] Katsouleas, T. and Mori, W. B. Wave-breaking amplitude of relativistic oscillations in thermal plasma. *Physical Review Letters*, 61(1): 90-93, 1988.

[25] Shukla, M. K. and Avinash, K. Equilibrium configuration of self-gravitating charged dust clouds: Particle approach. *Physics of Plasmas*, 26:013701, 2019.

[26] Shukla, M. K., Avinash, K., Mukherjee, R., and Ganesh, R. Isothermal Equation of State of Three Dimensional Yukawa Gas. *Physics of Plasmas*, 24, 113704, 2017.

[27] Koester, D. White dwarfs: Recent developments. *The Astronomy and Astrophysics Review*, 11: 33–66, 2002.

[28] Livio, M. and Pringle, J. E. The rotation rates of white dwarfs and pulsars. *The Astrophysical Journal*, 505(1): 339-343, 1988.

[29] Ferrario, L. and Wickramasinghe, D. T. Magnetic Fields and Rotation of Compact Stars. In 14th European Workshop on White Dwarfs, APS Conference Series, volume 334, pages 281-284, Kiel, Germany, 2005.

[30] Haque, Q. Drift and ion acoustic waves in an inhomogeneous electron-positron-ion plasma with temperature degeneracy and exchange-correlation effects. *Results in Physics*, 18:103287, 2020.

[31] Lang, K. R. *Essential Astrophysics*. Springer, New York, 2013.

[32] Córsico, A. H., Uzundag, M., Kepler, S. O., Althaus, L. G., Silvotti, R., Baran, A. S., Vučković, M., Werner, K., Bell, K. J., and M. Higgins, M. Pulsating hydrogen-deficient white dwarfs and pre-white dwarfs observed with TESS. Asteroseismology of the GW Vir stars RX J2117+3412, HS 2324+3944, NGC 6905, NGC 1501, NGC 2371, and K 1-16. *Astronomy and Astrophysics*, 645:A117, 2021.

[33] Camenzind, M. *Compact Objects in Astrophysics: White Dwarfs, Neutron Stars and Black Holes*. Springer, New York, 2007.

[34] Sadiq, S., Mahmood, S., and Haque, Q. Nonlinear Periodic Ion Acoustic Waves in a Relativistic Plasma with Isothermal Electrons and Cold Ions. *Journal of the Physical Society of Japan*. 90: 03450, 2021.

[35] Bespalov, P. A. and Savina, O. N. An excitation mechanism of electromagnetic pulses by relativistic electrons in the brown dwarfs rarefied magnetosphere. *Monthly Notices of the Royal Astronomical Society*, 480 (4):4761-4765, 2018.

[36] Abdikian, A., Farahani, S. V., and Hussain, S. The characteristics of daughter waves emerging from colliding solitary waves in astrophysical plasma media. *Monthly Notices of the Royal Astronomical Society*, 506(1):997-1006, 2021.

[37] El-Moniera, S.Y. and Atteya, A. Higher order corrections and temperature effects to ion acoustic shock waves in quantum degenerate electron-ion plasma. *Chinese Journal of Physics*:60 (2019), 695-708, 2019.

[38] Fitzpatrick, R. *Plasma Physics- An Introduction*. CRC Press, Boca Raton, 1st edition, 2014.

[39] Karmakar, P. K. and Gautam, H. Stability analysis of the gravito-electrostatic sheath-based solar plasma equilibrium. *Monthly Notices of the Royal Astronomical Society*, 460(3):2919-2932, 2016.

[40] Peng, Q-H., Liu, J-J., and Chou, C-K. New insight into the physical essence of pulsar glitch. *New Astronomy*, 90:101655, 2022.